



**University of  
Zurich**<sup>UZH</sup>

**Zurich Open Repository and  
Archive**

University of Zurich  
University Library  
Strickhofstrasse 39  
CH-8057 Zurich  
[www.zora.uzh.ch](http://www.zora.uzh.ch)

---

Year: 2015

---

## **Functional validation of mouse tyrosinase non-coding regulatory DNA elements by CRISPR–Cas9-mediated mutagenesis**

Seruggia, Davide ; Fernández, Almudena ; Cantero, Marta ; Pelczar, Pawel ; Montoliu, Lluís

**Abstract:** Newly developed genome-editing tools, such as the clustered regularly interspaced short palindromic repeat (CRISPR)-Cas9 system, allow simple and rapid genetic modification in most model organisms and human cell lines. Here, we report the production and analysis of mice carrying the inactivation via deletion of a genomic insulator, a key non-coding regulatory DNA element found 5' upstream of the mouse tyrosinase (Tyr) gene. Targeting sequences flanking this boundary in mouse fertilized eggs resulted in the efficient deletion or inversion of large intervening DNA fragments delineated by the RNA guides. The resulting genome-edited mice showed a dramatic decrease in Tyr gene expression as inferred from the evident decrease of coat pigmentation, thus supporting the functionality of this boundary sequence in vivo, at the endogenous locus. Several potential off-targets bearing sequence similarity with each of the two RNA guides used were analyzed and found to be largely intact. This study reports how non-coding DNA elements, even if located in repeat-rich genomic sequences, can be efficiently and functionally evaluated in vivo and, furthermore, it illustrates how the regulatory elements described by the ENCODE and EPIGENOME projects, in the mouse and human genomes, can be systematically validated

DOI: <https://doi.org/10.1093/nar/gkv375>

Posted at the Zurich Open Repository and Archive, University of Zurich

ZORA URL: <https://doi.org/10.5167/uzh-154853>

Journal Article

Published Version

Originally published at:

Seruggia, Davide; Fernández, Almudena; Cantero, Marta; Pelczar, Pawel; Montoliu, Lluís (2015). Functional validation of mouse tyrosinase non-coding regulatory DNA elements by CRISPR–Cas9-mediated mutagenesis. *Nucleic Acids Research*, 43(10):4855–4867.

DOI: <https://doi.org/10.1093/nar/gkv375>

# Functional validation of mouse *tyrosinase* non-coding regulatory DNA elements by CRISPR–Cas9-mediated mutagenesis

Davide Seruggia<sup>1,2</sup>, Almudena Fernández<sup>1,2</sup>, Marta Cantero<sup>1,2</sup>, Pawel Pelczar<sup>3</sup> and Lluís Montoliu<sup>1,2,\*</sup>

<sup>1</sup>Department of Molecular and Cellular Biology, National Centre for Biotechnology (CNB-CSIC), Campus Cantoblanco, Darwin 3, 28049 Madrid, Spain, <sup>2</sup>CIBERER-ISCIII, Madrid, Spain and <sup>3</sup>Institute of Laboratory Animal Science, University of Zurich, Zurich, Switzerland

Received March 08, 2015; Revised April 07, 2015; Accepted April 08, 2015

## ABSTRACT

Newly developed genome-editing tools, such as the clustered regularly interspaced short palindromic repeat (CRISPR)–Cas9 system, allow simple and rapid genetic modification in most model organisms and human cell lines. Here, we report the production and analysis of mice carrying the inactivation via deletion of a genomic insulator, a key non-coding regulatory DNA element found 5' upstream of the mouse *tyrosinase* (*Tyr*) gene. Targeting sequences flanking this boundary in mouse fertilized eggs resulted in the efficient deletion or inversion of large intervening DNA fragments delineated by the RNA guides. The resulting genome-edited mice showed a dramatic decrease in *Tyr* gene expression as inferred from the evident decrease of coat pigmentation, thus supporting the functionality of this boundary sequence *in vivo*, at the endogenous locus. Several potential off-targets bearing sequence similarity with each of the two RNA guides used were analyzed and found to be largely intact. This study reports how non-coding DNA elements, even if located in repeat-rich genomic sequences, can be efficiently and functionally evaluated *in vivo* and, furthermore, it illustrates how the regulatory elements described by the ENCODE and EPIGENOME projects, in the mouse and human genomes, can be systematically validated.

## INTRODUCTION

Non-coding DNA regulatory elements are composed of arrays of DNA–protein binding sites extending over tens to hundreds of base pairs that are occupied by multiple groups of transcription factors. DNA methylation, covalent mod-

ification of histone proteins and DNase I hypersensitivity profiles allow unbiased identification of such elements as regions of active chromatin that might be relevant in the regulation of different genes in a particular tissue or condition. Systematic ChIP-Sequencing (chromatin immunoprecipitation coupled with massive parallel sequencing) using antibodies specific for a variety of nuclear factors, applied to several human cell lines (1) and mouse tissues (2), served to identify cell type-specific regulatory elements accounting for almost 80% of the non-coding fraction of the genome. These studies, globally known as the ENCODE project (Encyclopaedia of DNA Elements; (3)) underline the rich proportion of functional elements existing within the non-coding areas of mammalian genomes. The recent publication of the human EPIGENOME project has provided additional evidence for the relevance of DNA regulatory elements in controlling gene expression (4). However, many functional experiments are required to unequivocally demonstrate the links between the observed biochemical chromatin features and the predicted biological function (5).

In the past years, the relevance of non-coding regions has been typically addressed, *in vivo*, using genomic-type transgenes (mostly bacterial and yeast artificial chromosomes, BACs and YACs; reviewed in (6)) carrying the inactivation of putative regulatory elements surrounded by tens to hundreds of kilo bases of genomic sequences of a suitable endogenous gene or coupled to a reporter gene (7–11). In this manner, large genomic fragments have been easily manipulated using homologous recombination in bacteria (12) and yeast (13) and then introduced into the mouse germline by standard procedures (14–15). However, variability is often observed between transgenic lines generated with BAC- or YAC-type transgenes, suggesting that position effects can influence transgene expression, even on large constructs (15–21). In addition, not all loci fit in such

\*To whom correspondence should be addressed. Tel: +34 915854844; Fax: +34 915854506; Email: montoliu@cnb.csic.es  
Present address: Pawel Pelczar, Center for Transgenic Models, University of Basel, Basel, Switzerland.

artificial chromosome-type transgenes, for example, large multi-gene syntenic blocks or gene clusters, whose transcriptional regulation programs during development are co-ordinated (22).

In mice and rats, non-coding regulatory elements can also be inactivated at the endogenous locus by gene targeting in embryonic stem (ES) cells, a routine and standardised process that relies on low-frequency homologous recombination events (23). Genetic manipulation of the endogenous locus will often result in a phenotype that truly reflects the relevance of the targeted sequence, either a coding gene or a regulatory element, mimicking disease conditions found in man (24–27). However, generating mouse models by gene targeting in ES cells is a lengthy procedure requiring several breeding steps to eventually bring the targeted allele from ES cells to the desired genetic background to investigate the phenotype. Furthermore, the presence of repetitive DNA sequences, often flanking regulatory elements, complicate the design of targeting vectors and can ultimately lead to suboptimal gene targeting (28). Indeed, we previously attempted and failed to inactivate the *Tyr* 5' regulatory DNA element analyzed in this current study by standard gene targeting in mouse ES cells, likely because of the repetitive nature of the DNA sequences surrounding this element ((29) and Victoria Tovar and Lluís Montoliu, unpublished).

After more than two decades of basic research (reviewed in (30)), RNA-guided genome editing has emerged as an alternative technique to achieve a wide variety of targeted genetic manipulations and CRISPR–Cas9-mediated mutagenesis has rapidly become the preferred approach in animal transgenesis (31). The combined microinjection of a single guide RNA (sgRNA) molecule specific for the target sequence and the RNA encoding the CRISPR-associated protein 9 (Cas9) drives the generation of double-strand breaks (DSBs) at the target site (32) with a frequency as high as 95% in mouse embryos (33). Thereafter, when a DSB is resolved through the non-homologous end-joining (NHEJ) repair pathway, several small insertion and deletions (*indels*) are introduced, often disrupting the coding sequence of a targeted gene. In the presence of a DNA template, either single or double stranded, subtle genetic modifications can be introduced through homologous recombination. Multiple target sites in the genome can be edited simultaneously by co-delivery of Cas9 and several sgRNAs (33). Furthermore, when two adjacent genomic sites are targeted, potentially triggering simultaneous DSBs, loss of the intervening DNA sequence can occur. Consequently, this approach can also be applied for producing large and targeted deletions (34).

Tyrosinase is the first and main enzyme in the melanin biosynthesis pathway (35–36). Mutations in *Tyr*, the gene encoding tyrosinase, result in hypopigmented phenotypes due to reduced melanin production in the two cell types where this gene is specifically expressed, namely, neural crest-derived melanocytes and retinal pigment epithelium (RPE) cells, derived from the optic cup (37). *Tyr* null mutants are unable to produce melanin and result in albinism, a rare genetic condition described in nearly all animals. In humans, mutations in the orthologous *TYR* locus are associated with oculocutaneous albinism type I (OCA1), the commonest form of albinism in Europe and America and one of

the 18 types of albinism (and genes) known for this group of rare diseases, whose common features, besides variable hypopigmentation, are the profound visual abnormalities (38).

Here, we report the inactivation, through deletion, of a key non-coding regulatory element, a genomic boundary located in the 5' region ~12 kb upstream of the mouse *Tyr* locus (7,29,39,40) using a CRISPR–Cas9 approach. We produced several founder mice using a combination of Cas9 and two sgRNAs targeting unique sequences flanking the *Tyr* 5' boundary. The genome-edited mice we obtained lacking this DNA sequence displayed a clear and robust phenotype, thus supporting the *in vivo* relevant function of this non-coding element at the endogenous locus.

## MATERIALS AND METHODS

### CRISPR–Cas9 plasmid and RNA preparation

Repeat-masked sequences in the region 5' upstream of the mouse *Tyr* gene were scanned using the online tool [crispr.mit.edu](http://crispr.mit.edu). Top scoring sgRNA sequences and related off-target sites were retrieved. CRISPR–Cas9 reagents were prepared as reported (41). Briefly, the Cas9 coding sequence was obtained from the hCas9 vector (Addgene, #41815) and PCR amplified with the oligonucleotides T7-Cas9Fw (which includes the T7 RNA polymerase promoter) and Cas9Rv (Supplementary Table S1). One microgram of purified PCR product was used for RNA *in vitro* transcription using the mMessage mMachine Ultra T7 Kit (Ambion). Two complementary oligonucleotides were designed carrying 20 bp of the target site and *Esp31*-compatible overhangs as reported previously, annealed *in vitro* and cloned by Golden Gate Cloning in the *Esp31* sites of the sgRNA expression vector MLM3636 (Addgene, #43860). A PCR product of the sgRNA cassette was used for RNA transcription using T7 RNA polymerase (Roche) with no further capping or polyA-tailing reactions. Both Cas9 and sgRNA were purified using NucAway Spin Columns (Ambion) and rehydrated in sterile RNase-free microinjection buffer (1 mM Tris–HCl pH 7.5, 0.1 mM EDTA pH 7.5).

### CRISPR–Cas9 RNA microinjection into mouse fertilized eggs

For microinjection, 35–50 ng/μl of Cas9 mRNA and 60–90 ng/μl of each sgRNA species were prepared in sterile RNase-free microinjection buffer (1 mM Tris–HCl pH 7.5; 0.1 mM EDTA pH 7.5), centrifuged for 30 min at 14 000 × g at 4°C and kept on ice until use. RNA molecules were co-microinjected into the cytoplasm of B6CBAF2 (Harlan; originated from B6CBAF1/OlaHsd) fertilized eggs. RNA was also delivered into the pronucleus to visually confirm the microinjection step. Additional mouse manipulations were performed following standard procedures (43). Founder animals were bred to albino outbred HsdWin:NMRI (Harlan) mice, the reference albino genetic background used in all previous *Tyr* transgenic mouse studies (7). TYRINS5 mouse lines were maintained in albino outbred HsdWin:NMRI background. Whole-mounted retinæ from adult mice were prepared as described (9). Melanin contents in skin and eye extracts

were estimated as reported before (43), measuring it as optical density (OD) at 492 nm (44) and expressed per gram of fresh tissue. Statistical analyses (One-way ANOVA with *post-hoc* Bonferroni correction) were carried out using IBM SPSS Statistics 21 software.

In this study, all genome-edited mouse lines were named as TYRINS5# followed by a number corresponding to the founder they were derived from. However, the correct nomenclature for these newly generated mouse lines is stock-*Tyr<sup>emXLmon</sup>*, where 'X' is the corresponding ordinal number for each TYRINS5 mouse line, as recommended by the International Committee on Standardized Genetic Nomenclature for Mice (Mouse Genome Informatics: <http://www.informatics.jax.org/mgihome/nomen/index.shtml>).

All the procedures that required the use of animals complied with Spanish and European legislation concerning vivisection and the use of genetically modified organisms, and the CSIC Ethics Committees on Animal Experimentation approved the protocols.

### T7 endonuclease I assay (T7 assay)

A 400–700 bp fragment centred on the target site was amplified by PCR in a 25 µl reaction. The PCR product was melted and cooled in a thermocycler as reported (41) to favor the formation of heteroduplexes. Ten microliters of PCR product were digested with 0.3 µl of T7 Endonuclease I (NEB) in a 20 µl reaction for 30 min at 37°C and resolved on a 2% TBE–agarose gel. All oligonucleotides used in this study are detailed in Supplementary Table S1.

## RESULTS

### Deletion of the *Tyr* 5' boundary results in a dramatic reduction in coat color pigmentation

We aimed to delete the mouse *Tyr* 5' boundary element (Figure 1; boxes A and B; (29)) by CRISPR–Cas9-mediated DNA cleavage. This regulatory element is also marked by reported H3K4me1 and p300 ChIP profiles in mouse melanocytes (Figure 1B; (42)). To obtain the desired 1.2 kb deletion, we microinjected pigmented (B6CBAF2) mouse fertilized eggs with Cas9 mRNA and two sgRNAs (5'0 and 5'5, Figure 1C) targeting flanking sequences located upstream and downstream of the mouse *Tyr* 5' boundary element following described procedures (41). We obtained a total of 64 live pups (Table 1), four of them already showing obvious alterations in coat color pigmentation (Figure 2A–D), suggesting that both copies of the *Tyr* 5' boundary element have been deleted. Each of these four founder mouse lines initially showed distinct levels and patterns of pigmentation, likely representing variable mosaicism. Indeed, upon breeding each founder animal with albino outbred Hsd-Win:NMRI mice (our reference albino strain used in all previous *Tyr* functional studies; (7)), all F1 progenies inheriting the edited alleles showed the same and robust phenotype, which presented as a uniform weakly-pigmented light grey coat color (Figure 2E–H). We termed each of these genome-edited mouse lines as TYRINS5 followed by an ordinal number (#N) corresponding to the founder mouse (see 'Materials and methods' section for the standard nomenclature of all genome-edited mice).

### Deletions of variable size produced by targeting adjacent sequences

Chromosomal deletions could be observed in 19 (30%) mouse lines by systematic T7 endonuclease I assay (T7 assay, see 'Materials and methods' section) and PCR evaluation of all 64 founder mice generated (Table 2). Notably, and most likely as a consequence of NHEJ, partial deletions as well as deletions spanning outside the targeted region were also observed in six mouse lines: TYRINS5#3, #13, #18b, #57, #60 and #62 (Figure 1B). For example, in founder TYRINS5#13, the deletion extends approximately 500 bp upstream of the sgRNA 5'0. In other mouse lines, large deletions appear to have been generated by a single DSB followed by extensive exonuclease activity. In fact, we could not observe *indels* associated with the sgRNA 5'5 site after sequencing the partial deletions in founder mouse lines TYRINS5#8 and TYRINS5#18b (Supplementary Figure S1). Regarding the mouse lines carrying deletions of the expected size (TYRINS5#6, #11, #18a, #20, #21, #30, #35, #48 and #53; Figure 1B), subsequent and systematic cloning and sequencing approaches confirmed that the deletion breakpoint occurred in close proximity to the sgRNA target sites and, frequently, 3 bp upstream to the Protospacer Adjacent Motif (PAM) as previously reported (32). In two cases (founder mice TYRINS5#18 and TYRINS5#60, Figure 1C), we observed two distinct deletions (TYRINS5#18a and #18b; TYRINS5#60a and #60b) occurring in the same founder animal, which later segregated independently in the F1 generation, resulting in a total of twenty one different deletions generated. We chose ten of the twenty one mouse lines carrying deletions produced by CRISPR–Cas9 for further analysis (TYRINS5#8, #11, #13, #18a, #18b, #30, #35, #50 and #60a and #60b). All eight founder mice carrying deletions transmitted these ten edited alleles through the germ line (Table 3). We could confirm a Mendelian inheritance pattern in four of these 10 mouse lines, whereas mosaicism was observed in the remaining mouse lines (45).

### DSBs generated by Cas9 at adjacent sites can also cause chromosomal inversions

The inversion of the intervening DNA is another possible resolution of two distal DSBs as previously reported in cultured cells (46) or in zebrafish (47). We therefore investigated whether chromosomal inversions could have been produced in our experimental model. The majority of founder mice generated in our experimental approach (52/64, 81%) carried mutations affecting one of the two target sites, or both, or were associated with deletions or inversions (Table 2). Indeed, we could detect specific inversion of the targeted sequence in seven animals by PCR using a forward primer mapping outside the targeted region (LCRdelFw) in combination with a second forward primer mapping inside the targeted region (67\_Fw) (Figure 3A and B and Supplementary Figure S2). Cloning and sequencing procedures confirmed these results. The inversion breakpoints were found in the immediate proximity of sgRNA target sites and were often accompanied by *indels* (Figure 3C). To date, we have obtained germ line transmission of these inverted alleles only for two of the six tested founders



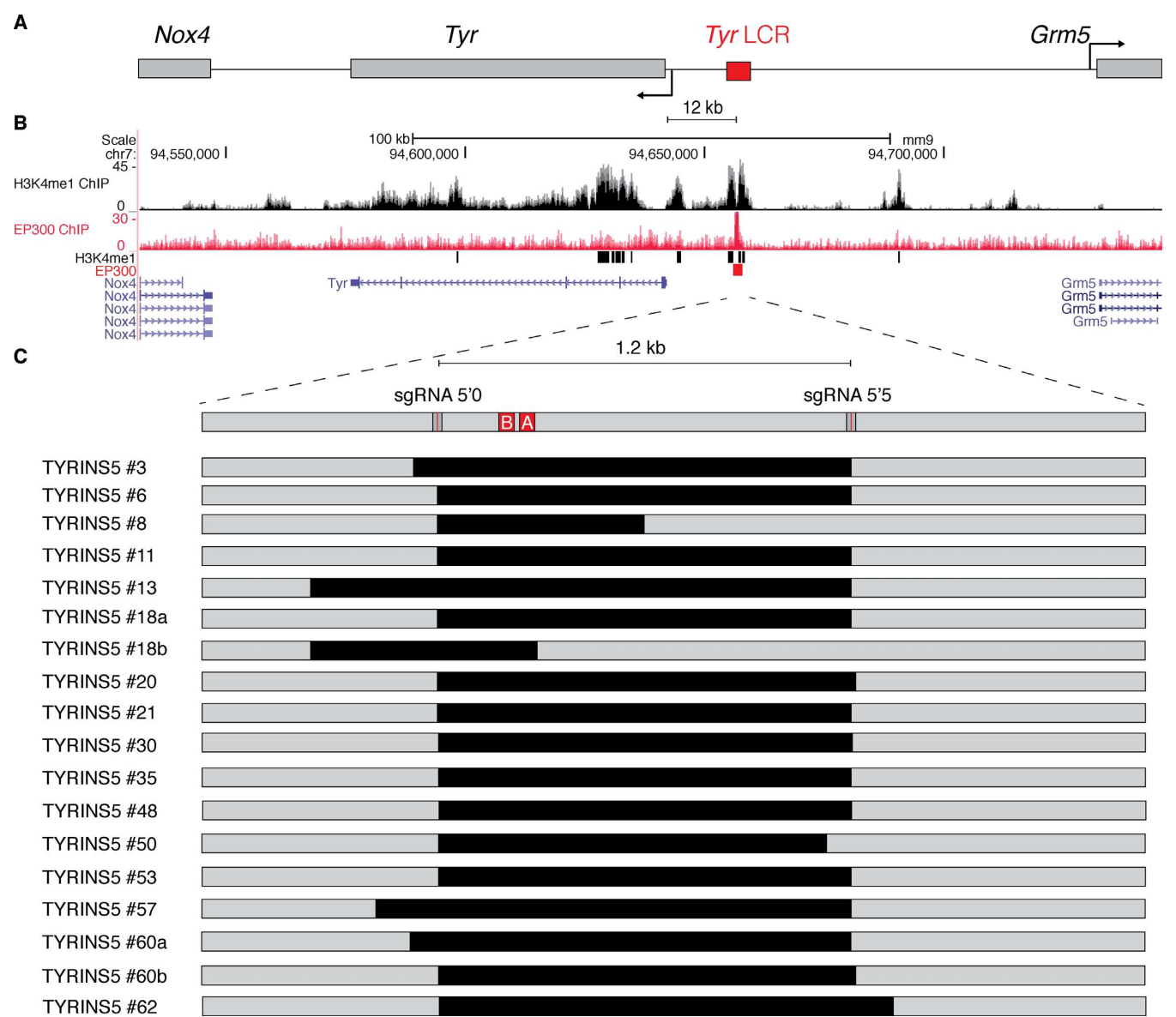


**Figure 1.** The mouse *Tyr* locus in its genomic location. Experimental design to delete the *Tyr* 5' boundary element by CRISPR–Cas9-mediated mutagenesis and chromosomal deletions found in founder animals. (A) The mouse *Tyr* locus in its genomic landscape flanked by *Nox4* and *Grm5* genes. The *Tyr* LCR (7) which includes the *Tyr* 5' boundary (29) is shown as a red box at ~12 kb from the *Tyr* promoter. (B) UCSC Genome browser tracks displaying H3K4me1 and p300 ChIP peaks around the *Tyr* locus in mouse melanocytic melan-a cells, adapted from reported results (42). (C) **Above:** Position of the *Tyr* 5' boundary core elements (A and B boxes, shown in red (29,39) and CRISPR sgRNA 5'0 and sgRNA 5'5 target sites, spaced 1.2 kb with respect to the *Tyr* locus). Simultaneous DSBs triggered by Cas9 nuclease at the sgRNA sites 5'0 and 5'5 will produce a 1.2 kb deletion. **Below:** Position and size of the deletions obtained. For each TYRINS5 edited mouse line, the deleted DNA region is indicated as a black box. In addition to the deletion of the expected size (1.2 kb), larger and smaller deletions were also observed. Two different deletions occurred in founders #18 and #60, here indicated as #18a, #18b and #60a, #60b.

**Table 1.** CRISPR–Cas9 RNA microinjection into B6CBAF2 fertilized eggs

RNA concentration	Microinjected mouse fertilized eggs	Transferred mouse embryos (% microinjected)	Number of fosters used	Live pups obtained (% transferred)	Positive mouse lines (deletions) (% live pups)
35 ng/μl Cas9	163	86 (52%)	5	31 (36%)	7 (23%)
60 ng/μl sgRNA					
50 ng/μl Cas9	225	99 (44%)	7	33 (33%)	12 (36%)
90 ng/μl sgRNA					
TOTAL	388	185 (47%)	12	64 (35%)	19 (30%)

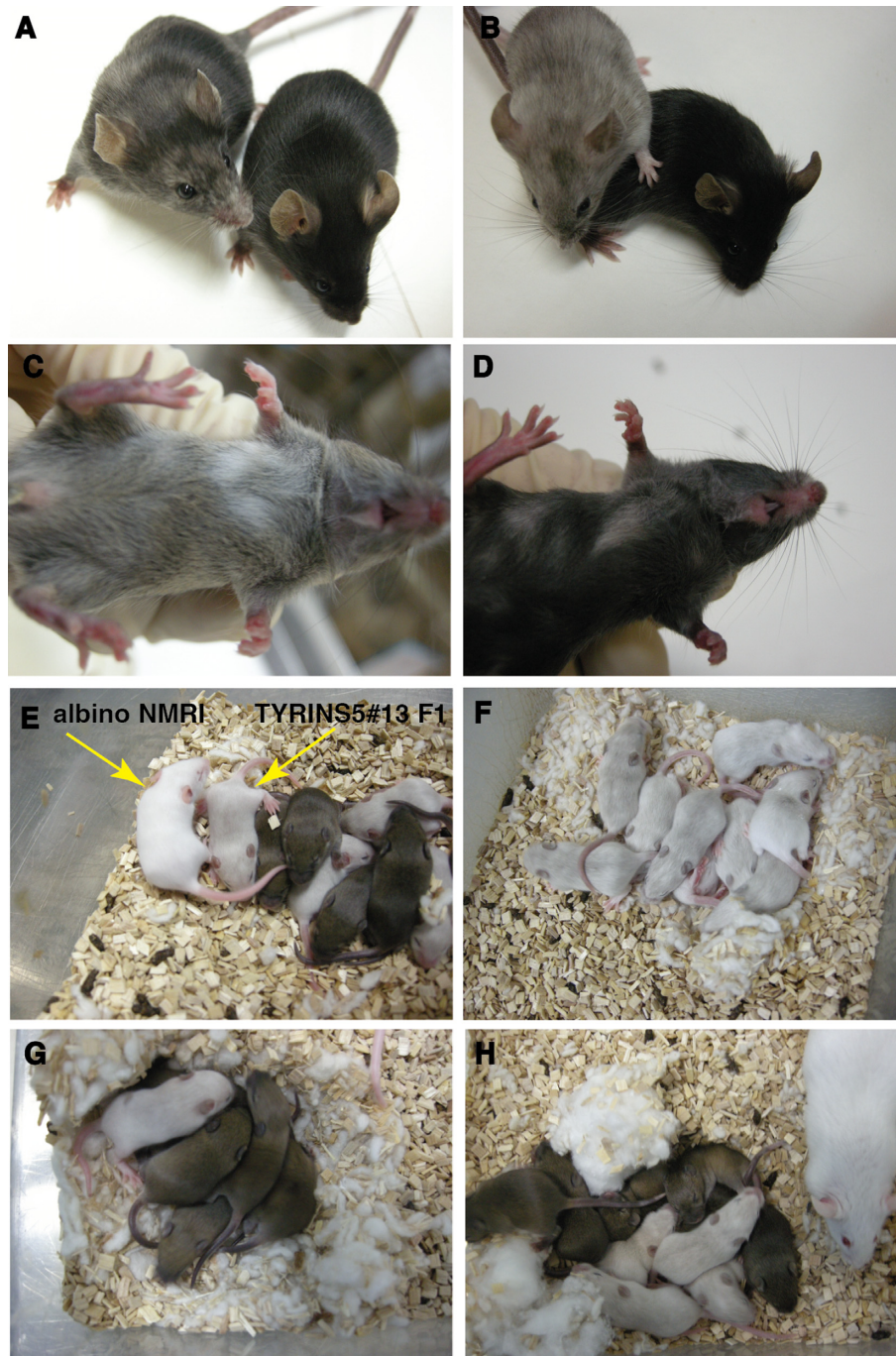


**Figure 2.** Alterations in coat color pigmentation in founder animals and their progeny. (A) Coat color alterations of founder mouse TYRINS5#11 (left) with a non-transgenic pigmented littermate. (B) Founder mouse TYRINS5#18 (left) is shown with a non-transgenic littermate: a lighter coat color is observed compared with founder TYRINS5#11, indicating a weaker degree of mosaicism. (C) Founder mouse TYRINS5#35 shows hypopigmented patches in the belly. (D) Founder mouse TYRINS5#60, strongly pigmented and, likely suggesting a higher degree of mosaicism. (E) F1 animals obtained by breeding founder TYRINS5#13 with albino outbred HsdWin:NMRI wild-type mice. A strong reduction of coat color pigmentation is observed in mice carrying the deletion of the *Tyr* 5' boundary element. Notably, pigment is not fully absent, as in the case of albino mice (indicated with yellow arrows), but dramatically reduced when compared with pigmented, wild-type animals. (F) All F1 progeny obtained from founder TYRINS5#18 (shown in B) show uniformly reduced pigmentation, indicating that both copies of the *Tyr* 5' boundary element were deleted in this founder. (G) F1 mouse derived from founder TYRINS5#19, carrying an inversion of the intervening *Tyr* 5' sequence. In this case, the inversion was transmitted to just one individual, showing the same phenotype as those carrying a deletion of the same DNA sequence (panels E, F and H). (H) F1 progeny of the founder TYRINS5#60 (shown in D). The individuals that inherited the deletion of the *Tyr* 5' boundary element show a clear and robust reduction in coat color pigmentation.

**Table 2.** Types of mutations observed among the 64 TYRINS5 founder mice generated

RNA concentration	T7 Endo I assay <sup>a</sup> sgRNA 5'0	T7 Endo I assay <sup>a</sup> sgRNA 5'5	Deletions	Inversions	No mutations
35 ng/μl Cas9	11/31 (35%)	18/31 (58%)	7/31 (23%)	2/31 (6%)	8/31 (26%)
60 ng/μl sgRNA					
50 ng/μl Cas9	12/33 (36%)	22/33 (67%)	12/33 (36%)	5/33 (15%)	4/33 (12%)
90 ng/μl sgRNA					
Total	23/64 (36%)	40/64 (62%)	19/64 (30%)	7/64 (11%)	12/64 (19%)

<sup>a</sup>T7 Endo I assay = T7 Endonuclease I assay.

**Table 3.** Germline transmission of TYRINS5 mouse lines carrying deletions and inversions

Founder mouse line	Type of mutation	Edited mice/all F1 mice (percentage)	Germline transmission, inheritance type <sup>a</sup>
TYRINS5#8	0.7 kb deletion	14/35 (40%)	Yes, Mendelian
TYRINS5#11	1.2 kb deletion	1/27 (4%)	Yes, non-Mendelian
TYRINS5#13	1.2 kb deletion	8/26 (31%)	Yes, non-Mendelian
TYRINS5#18a	1.2 kb deletion	6/9 (66%)	Yes, Mendelian
TYRINS5#18b	0.7 kb deletion	3/9 (33%)	Yes, Mendelian
TYRINS5#30	1.2 kb deletion	3/37 (8%)	Yes, non-Mendelian
TYRINS5#35	1.2 kb deletion	3/21 (14%)	Yes, non-Mendelian
TYRINS5#50	1.2 kb deletion	7/23 (30%)	Yes, Mendelian
TYRINS5#60a	1.2 kb deletion	2/21 (10%)	Yes, non-Mendelian
TYRINS5#60b	1.2 kb deletion	6/21 (29%)	Yes, non-Mendelian
TYRINS5#19	1.2 kb inversion	2/17 (12%)	Yes, non-Mendelian
TYRINS5#23	1.2 kb inversion	0/14 (0%)	No
TYRINS5#30	1.2 kb inversion	0/37 (0%)	No
TYRINS5#31	1.2 kb inversion	0/42 (0%)	No
TYRINS5#41	1.2 kb inversion	7/17 (41%)	Yes, Mendelian
TYRINS5#60	1.2 kb inversion	0/21 (0%)	No

<sup>a</sup>Mendelian inheritance tested by chi-square test with the help of Mendel program (45).

(Table 3), and only in one case through a Mendelian ratio. These results suggest that this genomic rearrangement might have occurred later in embryo development, therefore associating with an increased mosaicism and resulting in weaker germ line contribution. Interestingly, we observed alterations in coat color pigmentation in the two mouse lines carrying the inverted *Tyr* 5' boundary (Figure 2H), resembling the phenotype seen in mice carrying deleted alleles (Figure 2E-G). This altered coat color pattern is also similar to that of the *chinchilla-mottled* (*Tyr<sup>c-m</sup>*) mouse mutant, a spontaneous *Tyr* mutant allele that carries a gross genomic inversion involving the *Tyr* 5' upstream region including the *Tyr* 5' boundary element (48,49).

Assessing the overall mutagenesis rate

Our main goal was to produce a targeted deletion by triggering two simultaneous DSBs at adjacent sites in the genome. Nevertheless, to assess the overall mutagenesis efficiency we achieved in this CRISPR–Cas9 genome editing protocol *in vivo*, we decided to systematically analyze the DNA sequence at both target sites (5'0 and 5'5) for all 64 pups obtained (Figure 1B and Table 2). We amplified DNA sequences flanking each of the two sgRNA target sites by PCR and digested the resulting PCR products with the mismatch-sensitive T7 Endonuclease I enzyme ('T7 assay'; as described in (41)) (Supplementary Figure S3). Analysis of agarose electrophoresis gels indicated that 36% of the animals presented *indel* mutations at the sgRNA 5'0 site and 62% carried *indels* at the sgRNA 5'5 site (Table 2). In addition, 25% of the founder animals were double positive in

the two T7 assays, in the absence of large deletions, suggesting that DSBs and the associated repair mechanisms may have not occurred synchronously. As many as 44% of the edited founder mice generated showed the typical CRISPR–Cas9 scar at only one of the two targeted sites (as was later confirmed by cloning and sequencing of PCR products). Twelve animals (19%) did not show any gross mutations that could be detected by the T7 assay. Next, we cloned and sequenced each targeted region. Most of the observed *indels* accumulated around the PAM motif. We also observed larger deletions induced by a single DSB, as previously reported (50). In summary, considering all animals analyzed, we could identify a variety of edited alleles triggered by sgRNAs 5'0 and 5'5 and, in many cases, co-segregating in the same mosaic founder mice, with the median size for the observed deletion being 9 bp (Supplementary Figure S4).

Analysis of potential off-target sites

Several independent laboratories have reported that CRISPR–Cas9 approaches *in vitro* can efficiently trigger DSBs at DNA regions with sequences that share similarity with the intended target site (51–53). We therefore evaluated whether our experimental design might have triggered alterations in other similar genomic locations. Thus, we retrieved genomic regions carrying high sequence similarity with either one of the two sgRNA target sites used according to the predicted sequences given by the algorithm we employed (online tool [crispr.mit.edu](http://crispr.mit.edu)) (Table 4). The three most similar predicted DNA sequences corresponding to each of the two selected sgRNAs (5'0



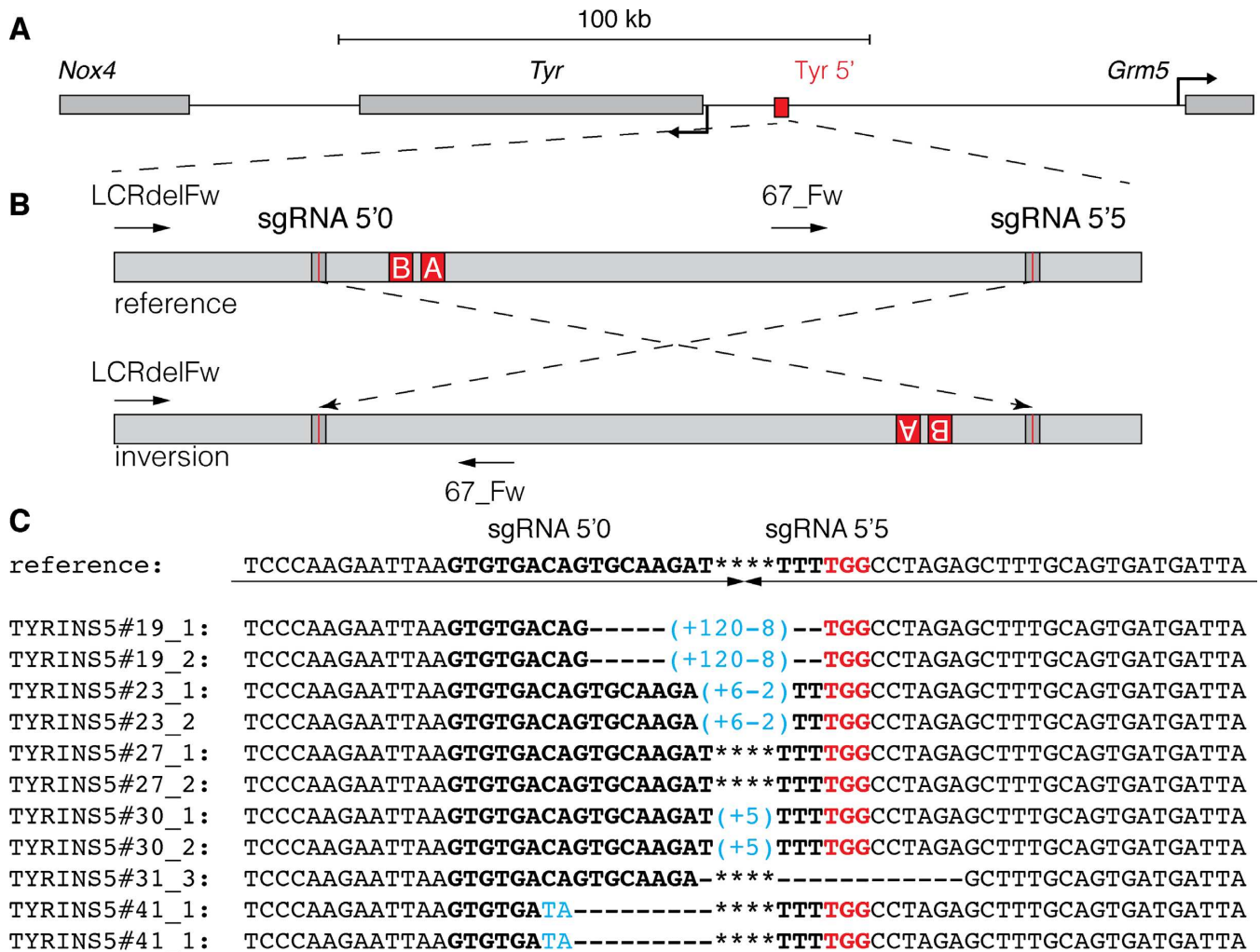


**Figure 3.** Chromosomal inversions generated by targeting two adjacent sites. **(A)** Scheme of the mouse *Tyr* locus. **(B)** Simultaneous cleavage at the sgRNA sites 5'0 and 5'5 can also trigger the inversion of the intervening DNA. Inversions can be detected using two oligonucleotides (LCRdelFw and 67.Fw) annealing on the same DNA strand. **(C)** Confirmation by cloning and Sanger sequencing of the different chromosomal inversion observed. *Indels* are found at the junction. CRISPR target sites are shown in bold, PAM motif is shown in red. The four asterisks indicate the inversion breakpoint. Deleted nucleotides are indicated as dashes; inserted bases are shown in blue.

and 5'5) were amplified by PCR and analyzed by the T7 assay in all 64 founder animals. The six loci were found to be mostly unmodified in the vast majority of animals (Supplementary Figures S5 and S6). We detected faint digested DNA products in very few animals in the T7 assay (Supplementary Figures S5 and S6, indicated with arrows); however, upon cloning and sequencing these selected PCR products, we failed to detect any obvious off-target mutation in any of the six additional genomic locations investigated (Supplementary Figure S7).

### An allelic series allows the functional identification of the core element of the *Tyr* 5' boundary

We have obtained multiple mouse lines lacking the specific intervening DNA region by targeting two adjacent sequences flanking the *Tyr* 5' boundary element (Figure 1B). Unexpectedly, we also obtained founder animals in which the deleted DNA sequence was found to be shorter, where

only a part of the targeted region has been eliminated, or larger, extending outside the intended region (Figure 1B). Nevertheless, irrespective of the deleted allele, the observed coat color phenotype for all these lines is indistinguishable (Figures 2E–G and 4A). Similarly, melanin contents in skin and eye extracts are comparable across independent lines (Figure 4C and D). We therefore decided to compare and align the DNA sequences of all the different alleles generated in order to genetically map the core sequence (deleted in common in all these lines) that would be responsible for the observed phenotype. The genetic analysis for this allelic series indicates that a 410 bp sequence (chr7: 94 656 561–94 656 970, mouse genome assembly NCBI m37 mm9) could be considered the core of the *Tyr* 5' boundary element (Figure 4B). The deletion of additional surrounding DNA sequences did not further alter the grey coat color pigmentation already observed in animals carrying smaller DNA deletions, including this core element. Interestingly, the core DNA element inferred from this functional genetic analysis



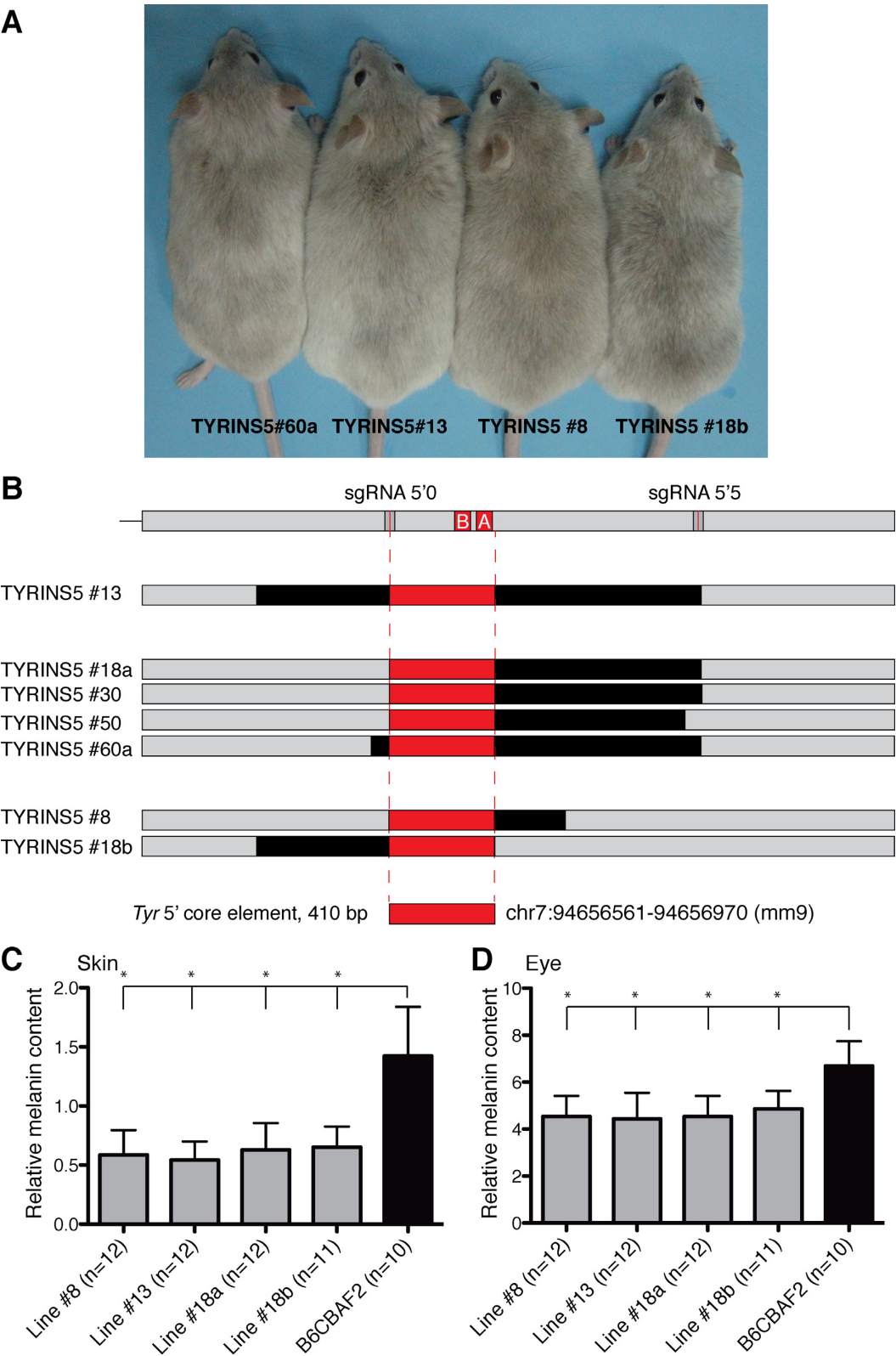


**Figure 4.** Genetic mapping of the *Tyr* 5' boundary core sequence. (A) F1 individuals from different TYRINS5 mouse lines (indicated below) carrying deleted alleles of different size but showing comparable coat color patterns. (B) Scheme illustrating a genomic sequence alignment of the distinct deletion alleles generated in this study, associated with mice displaying the most similar phenotype. The comparison of all deleted sequences allows the identification of a core element for the *Tyr* 5' boundary sequence (410 bp), shown in red, which encompasses the A and B boxes previously identified (29,39), and is likely responsible for the correct activation of *Tyr* in skin melanocytes *in vivo*. The coordinates of the red core element are indicated (Assembly NCBI m37/UCSC mm9). These coordinates correspond to chr7:87508051–87508460 in the newest mouse genome assembly GRCm38.p3 mm10. Melanin contents in the skin (C) and eye (D) of four different TYRINS5 mouse lines. (\**P* < 0.05, one-way ANOVA with *post-hoc* Bonferroni correction).

**Table 4.** Predicted off-target sites

Target site <sup>a</sup>	DNA sequence <sup>b</sup>	Genomic coordinates <sup>c</sup>	Feature (gene)
5'0 reference	GTGTGACAGTGCAAGATAACAGG	chr7: 94,656,546 - 94,656,568	Intergenic ( <i>Tyr</i> )
5'0-OT1	CTGT <u>C</u> ACAGAA <u>C</u> AAGATAACCGG	chr6: 99,084,014 - 99,084,036	intronic ( <i>Foxp1</i> )
5'0-OT2	GGGAGACTGTGCAAGATAAGGGG	chrX: 69,682,563 - 69,682,585	intronic ( <i>Gabra3</i> )
5'0-OT3	TTTTGACAGAGCAAGATAAA <u>T</u> GG	chr3: 60,502,350 - 60,502,362	intergenic
5'5 reference	GTGATAAAACTAGGCAATT <u>T</u> GG	chr7: 94,657,775 - 94,657,797	Intergenic ( <i>Tyr</i> )
5'5-OT1	CAGATAAAAGCAGGCAATTTTGG	chr1: 9,300,003 - 9,300,025	Intergenic
5'5-OT2	GAGCAAAAACTTGGCAATTTGGG	chr19: 31,071,409 - 31,071,431	Intronic ( <i>Prkg1</i> )
5'5-OT3	GTATTAATAATGAGGCAATTTGGG	chr14: 112,763,119 - 112,763,141	Intergenic

<sup>a</sup>OT = Off-target.<sup>b</sup>Nucleotides that differ from the reference sequence at the corresponding target site are shown underlined.<sup>c</sup>PAM sequence (NGG) shown in bold Assembly NCBI37/UCSCmm9.

sis at the endogenous *Tyr* locus is in good agreement and largely reflects previous findings obtained *in vitro* (29,39) and *in vivo* (7,9,39) using a variety of experimental strategies and transgenes. We further confirmed the similarity of the obtained mouse phenotypes by measuring the melanin content in skin and eye extracts whose contents were estimated in 42% and 69% of that of the wild-type pigmented littermates, respectively (Figure 4C and D). No statistically significant differences were observed among independent TYRINS5-edited mouse lines, whereas statistically significant differences were observed between any of the edited mouse lines and the wild-type pigmented animals.

#### Comparative analysis of TYRINS5-edited mice with YAC *Tyr* transgenic mice

The comparison of genome-edited mouse lines carrying a targeted inactivation of the 5' *Tyr* boundary (this work) with other mouse transgenic lines bearing similar deletions within large chromosome-type genomic transgenes reveals interesting but fundamental differences. The absence of the *Tyr* 5' boundary element in YRT4 (7), or its targeted deletion in YRT5 (7) and  $\Delta$ LCR (18) YAC transgenic mice, results in a strong reduction of *Tyr* gene expression in neural crest-derived melanocytes, as demonstrated by a dramatic reduction in coat color pigmentation (almost albino-like), associated with strongly variegated expression (9) (Figure 5A). In contrast, the reduced coat color phenotype observed in all targeted TYRINS5 lines is milder, uniformly light grey, and without signs of variegation (Figures 4A and 5A). Additionally, a more severe phenotype is observed in the eyes of YRT4 and  $\Delta$ LCR YAC transgenic mice, where a profound loss of pigment is obvious in choroidal melanocytes and strong variegation is observed at the RPE cell layer (9,18) (Figure 5C). In contrast, the expression of *Tyr* at the RPE cell layer appears unaffected in TYRINS5 mice in all analyzed lines, without signs of variegation, and the loss of *Tyr* expression in the choroid is less marked (Figure 5B), as it can also be inferred from eye melanin content measurements (Figure 4D).

## DISCUSSION

Here, we propose a simple strategy to functionally validate the relevance of non-coding regulatory elements in the mouse genome, *in vivo*. We have applied CRISPR-Cas9-

mediated mutagenesis tools to inactivate, via deletion, a key regulatory sequence identified in the mouse *Tyr* gene (48).

We previously reported a DNase hypersensitive (HS) site, located at ~12 kb 5'-upstream of the mouse *Tyr* transcription start site (TSS), associated with a melanocyte-specific enhancer that was required for the correct expression of the *Tyr* gene (39). The deletion or inactivation of this element, in the context of YAC transgenesis, produced mice displaying variegation with severely reduced coat color pigmentation, supporting the notion that this key element was acting as a Locus Control Region (LCR) (7)). Homologous sequences to this mouse *Tyr* 5' element were also found within the 5' end of the human *TYR* locus, suggesting that mutations in this element could also impair the function of the human *TYR* gene (54). Traditional molecular diagnosis efforts for OCA1 patients regularly fail to detect all *TYR* mutations, beyond coding, promoter and limited intronic DNA sequences routinely explored. Consequently, it has been repeatedly suggested that mutations in non-coding regions could be responsible for some of these unknown non-functional *TYR* alleles (38,55,56). Interestingly, the recent human epigenome data released for many cellular types, including skin melanocytes, describes a regulatory element (a DNase HS) located at ~10 kb 5' upstream of the human *TYR* gene promoter ((4); Supplementary Figure S8) at the same genomic location as was previously predicted (54). Until now, the direct relevance of *TYR* or *Tyr* regulatory elements could not be adequately studied at the endogenous loci. Instead, their role had to be inferred from results obtained using diverse standard and chromosome-type transgenes in mice (17,35).

Further studies revealed that the *Tyr* LCR had properties typical of genomic boundaries or insulators (57), including the capacity of establishing barriers that prevent spreading of heterochromatin and epigenetic silencing (29), and enhancer-blocking activity (40). The function of insulators is rather complex and strictly dependent on the interactions with other proximal and distal sequences in the genomic locus (43,58–60). The context-dependent activity of insulators should be therefore characterized in their native chromosomal context by gene targeting. However, the presence of repetitive sequences surrounding the *Tyr* 5' boundary element (29) invalidated the application of standard gene targeting approaches. As an alternative, we decided to use CRISPR-Cas9-mediated mutagenesis to overcome the limitations of classical gene targeting strategies.



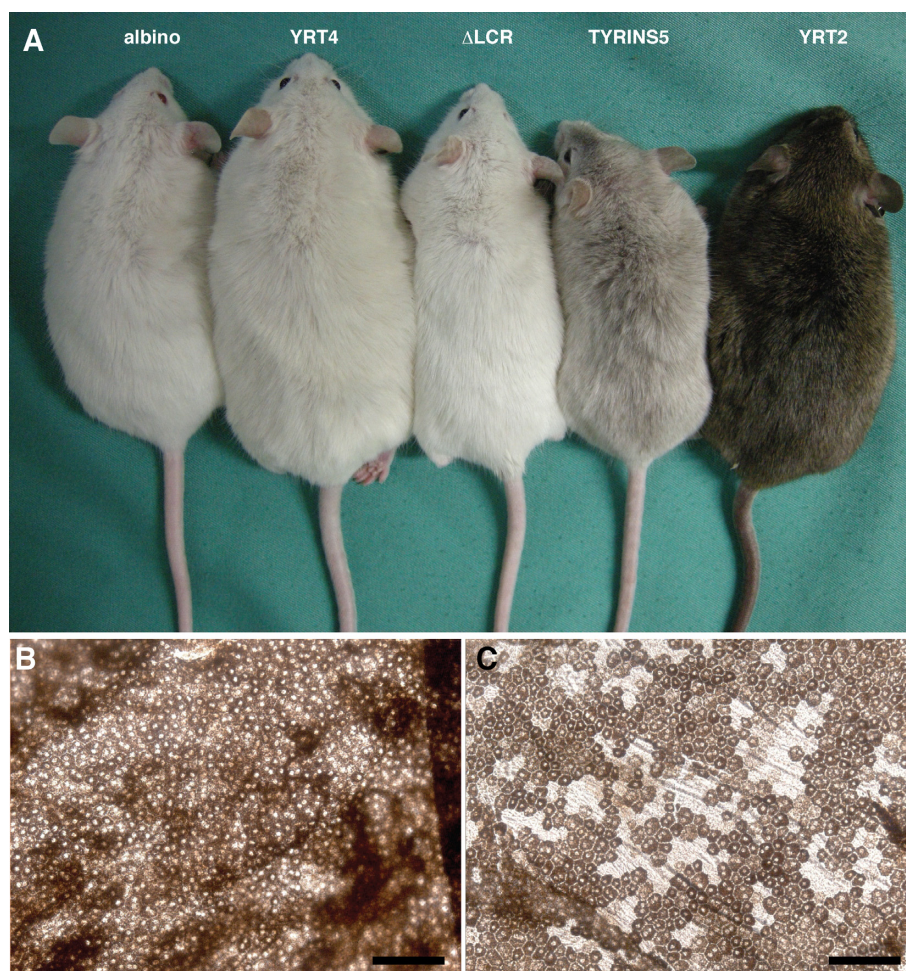


**Figure 5.** Inactivation of the *Tyr* 5' boundary element at the endogenous locus and in modified YAC *Tyr* transgenes. (A) Distinct *Tyr* mouse models, both transgenic (YAC YRT4 (7); YAC  $\Delta$ LCR (18) and genome-edited (TYRINS5) individuals, carrying the inactivation of the *Tyr* 5' boundary element presented along with albino outbred HsdWin:NMRI mice and fully pigmented YAC YRT2 transgenic mice carrying the entire *Tyr* expression domain (63). The coat color of  $\Delta$ LCR and YRT4 YAC transgenic mice is almost indistinguishable from albino mice due to a strongly variegated *Tyr* expression, but eyes are pigmented. In contrast, the coat color of the TYRINS5 edited mouse is light gray. (B) Whole-mounted retinæ obtained from a TYRINS5 edited mouse. (C) Whole-mounted retinæ obtained from a  $\Delta$ LCR transgenic mouse. Variegation is observed in  $\Delta$ LCR mice, at the RPE cell layer, whereas variegation is absent in TYRINS5 mice. In addition, a more severe loss of pigmentation at underlying choroidal melanocytes is observed in  $\Delta$ LCR as compared with TYRINS5 mice. Scale bars in (B) and (C) panels correspond to 50  $\mu$ m.

Similar approaches have been recently reported to address the role of a distal *Sox2* enhancer in mouse ES cells (5). Endonuclease-mediated deletions, using Transcription Activator-Like Effector Nucleases (TALENs) and Zinc-Finger Nucleases (ZFN), have been described in zebrafish (61). CRISPR–Cas9 was also used to characterize mutations found at the distal enhancer of the *TALI* oncogene in human tumor cell lines (62). Additionally, mouse models were generated using CRISPR–Cas9 in mouse ES cells to reproduce structural variants, including deletions and inversions, found in human disease (63).

In this work, we report that defined deletions and inversions in non-coding regions can be efficiently generated *in vivo* by CRISPR–Cas9 approaches using sgRNAs directed to adjacent genomic target sites. CRISPR–Cas9 RNA species are injected into fertilized eggs where they generate mutations at the target sequences. These mutations are then efficiently transmitted through the germ line. Us-

ing this strategy, mouse embryos are exposed to a limited amount of Cas9 nuclease for a short time, thus minimizing the risk of off-target mutations. Indeed, in our screen, no undesired mutations were detected at the six genomic loci highly similar to the targeted sequences under investigation. In contrast to this, approaches based on the delivery of CRISPR–Cas9 plasmids to somatic or ES cells may increase the associated risk of off-target mutations since exposure to the Cas9 nuclease is massive and prolonged (31).

Inactivation of the *Tyr* 5' boundary element in genomic-type transgenes resulted in a severe reduction in coat color pigmentation, pointing to a relevant role for this non-coding sequence (7). However, these results were based on ectopic chromosomal locations, where variables such as transgene integrity, copy number and integration site could affect the overall gene expression program (15–21). Because of this, our vision was to target this 5' boundary element directly at the *Tyr* endogenous locus, where we could unequiv-



ocally link this element to the observed phenotype without further uncontrolled variables. In actual fact, a comparative analysis of *Tyr* expression patterns in YAC *Tyr* transgenic mouse lines and TYRINS5 edited lines reveals fundamental differences in both melanocytes and RPE cells (Figures 4A, C, D, 5A, B and C). Deleting the *Tyr* 5' boundary appears to have a milder effect in skin and choroidal melanocytes and a more limited impact in RPE cells, suggesting that additional regulatory elements may be responsible for controlling *Tyr* gene expression in RPE cells. Indeed, the presence of RPE-specific regulatory elements further upstream had been previously proposed and investigated in mice using BAC *Tyr* transgenes engineered with a *lacZ* reporter gene and variable combinations of *Tyr* 5' genomic sequences (64).

The differences found in these two experimental approaches likely depend on the integration site and highlight the drawbacks/disadvantages of traditional transgenes, including large genomic-type transgenes, particularly when they lack relevant regulatory elements (7,9). Transgenesis with intact *Tyr* YAC transgenes such as YRT2 (65), encompassing the entire *Tyr* expression domain, result in mice that are virtually indistinguishable from wild-type agouti-pigmented mice. However, even with YRT2 transgenic mice, it was possible to detect very mild forms of variegation in RPE cells (Figure 3G in (9)). Therefore, large transgenes may behave differently at ectopic integration sites and may display somewhat different phenotypes compared with those associated with similar genomic alterations at the endogenous locus. The most common alteration seen in standard transgenic mice (and one of their most obvious limitations) is variegation, in which not all cells carrying a given transgene are able to express it adequately at ectopic locations. Also, variegation is more often observed in plasmid-type transgenes as compared with genomic-type transgenes (6). Conversely, targeted inactivation using nucleases allows unbiased characterization of cell type-specific regulatory elements, as recently achieved in human erythroid cells within the *BCL11A* (66) and *EZH1* (67) loci. Perhaps more importantly, inactivation of non-coding elements at their endogenous genomic locations allows, for the first time, investigation of changes in chromatin marks that may be associated with the loss of a genomic boundary. For example, our experimental model can now be used to investigate potential perturbations in the expression profiles of the neighboring *Nox4* and *Grm5* genes, which flank the *Tyr* locus in both human and mouse genomes, to assess whether the removal of a genomic boundary, such as the *Tyr* 5' element, disrupts the expression pattern scenario (Figure 1A). These analyses need to be addressed in homozygous mice. Similarly, the possible alteration of chromatin marks around the *Tyr* locus will have to be addressed in immortalized melanocytes, following experimental approaches described in previous studies (68).

We have produced several genome-edited mice carrying deletions of variable size around a non-coding regulatory element that display a strikingly similar phenotype (Figure 4A). The alignment of all distinct deletions highlights the core nucleotides functionally associated with this regulatory element (Figure 4B). In just one experiment, we could genetically map the relevant sequences associated with this regulatory element. A similar outcome using classical gene

targeting methods would have required multiple independent experiments. Hence, the uncertainty and uncontrolled nature of the deletion breakpoints edited alleles spontaneously generated by NHEJ can become a benefit for the *in vivo* characterization of non-coding regulatory elements.

In this work, we have investigated the role of the mouse *Tyr* 5' boundary element in its endogenous genomic location using a CRISPR–Cas9 approach. A series of deletions generated in mice allowed us to genetically map the relevant sequences associated with this boundary and to narrow down its function in the context of the regulation of *Tyr* gene expression. Interestingly, the *Tyr* 5' core element detected (Figure 4B) extends beyond the known A and B boxes (29,39), and includes potential binding sites for transcription factors Lmx1a and Lef-1 (as suggested by TRANSFAC and UniPROBE). Mutant mouse lines for these two transcription factors show alterations in coat color pigmentation (Montoliu L, Oetting WS, Bennett DC. Color Genes. April 2015. European Society for Pigment Cell Research. <http://www.espcr.org/micemut>), thus suggesting a potential relevance of these additional protein binding sites within the *Tyr* 5' regulatory element.

All genome-edited mice lacking this boundary displayed an overall reduction in coat color pigmentation, indicating a pivotal role for this regulatory element in skin melanocytes. However, RPE cells appeared largely unaffected, suggesting that this regulatory element is dispensable in this other cell type that expresses *Tyr*. These results finally overcome the variable phenotype traditionally observed with all previous transgenic *Tyr* mice based on plasmids or large genomic constructs. The differences observed between transgenic (at ectopic sites) and editing (at the endogenous site) approaches underscores the power and validity of systematic CRISPR–Cas9-mediated mutagenesis to functionally assess regulatory elements in non-coding sequences that have been discovered by the ENCODE and EPIGENOME projects. Moreover, functional analysis of regulatory elements, now feasible in animal models and cellular models of human disease, will likely increase our current understanding on the origin and underlying mechanisms of many pathologies of genetic origin.

## SUPPLEMENTARY DATA

Supplementary Data are available at NAR Online.

## ACKNOWLEDGEMENTS

The authors wish to thank the CNB-CBMSO Transgenic Facility, led by Belén Pintado, for the production of the genome-edited mice reported in this study; William J. Pavan and Stacie K. Loftus (NIH) for kindly providing melan-a ChIP-seq data; Irene Robles (UAM) for help with off-target sequence analyses; and Kenneth McCreath for editorial assistance.

## FUNDING

Spanish Ministry of Economy and Competitiveness (MINECO) [BIO2012-39980] to L.M.; Biomedical and Biological Sciences (BMBS) European Cooperation in Science and Technology (COST) action [BM1308 SALAAM]

to L.M.; La Caixa International PhD and EMBO Short Term Fellowship [AST140-2013] programs to D.S. Funding for open access charge: MINECO [BIO2012-39980] to L.M.

*Conflict of interest statement.* None declared.

## REFERENCES

1. Encode Project Consortium. (2012) An integrated encyclopedia of DNA elements in the human genome. *Nature*, **489**, 57–74.
2. Yue, F., Cheng, Y., Breschi, A., Vierstra, J., Wu, W., Ryba, T., Sandstrom, R., Ma, Z., Davis, C., Pope, B.D. *et al.* (2014) A comparative encyclopedia of DNA elements in the mouse genome. *Nature*, **515**, 355–364.
3. Birney, E. (2012) The making of ENCODE: lessons for big-data projects. *Nature*, **489**, 49–51.
4. Roadmap Epigenomics Consortium. (2015) Integrative analysis of 111 reference human epigenomes. *Nature*, **518**, 317–330.
5. Li, Y., Rivera, C.M., Ishii, H., Jin, F., Selvaraj, S., Lee, A.Y., Dixon, J.R. and Ren, B. (2014) CRISPR reveals a distal super-enhancer required for Sox2 expression in mouse embryonic stem cells. *PLoS One*, **9**, e114485.
6. Giraldo, P. and Montoliu, L. (2001) Size matters: use of YACs, BACs and PACs in transgenic animals. *Transgenic Res.*, **10**, 83–103.
7. Montoliu, L., Umland, T. and Schutz, G. (1996) A locus control region at -12 kb of the tyrosinase gene. *EMBO J.*, **15**, 6026–6034.
8. Peterson, K.R., Clegg, C.H., Navas, P.A., Norton, E.J., Kimbrough, T.G. and Stamatoiyannopoulos, G. (1996) Effect of deletion of 5' HS3 or 5' HS2 of the human beta-globin locus control region on the developmental regulation of globin gene expression in beta-globin locus yeast artificial chromosome transgenic mice. *Proc. Natl. Acad. Sci. U.S.A.*, **93**, 6605–6609.
9. Gimenez, E., Giraldo, P., Jeffery, G. and Montoliu, L. (2001) Variegated expression and delayed retinal pigmentation during development in transgenic mice with a deletion in the locus control region of the tyrosinase gene. *Genesis*, **30**, 21–25.
10. Horvath, L.M., Li, N. and Carrel, L. (2013) Deletion of an X-inactivation boundary disrupts adjacent gene silencing. *PLoS Genet.*, **9**, e1003952.
11. van den Boogaard, M., Smemo, S., Burnicka-Turek, O., Arnolds, D.E., van de Werken, H.J., Klous, P., McKean, D., Muehlschlegel, J.D., Moosmann, J., Toka, O. *et al.* (2014) A common genetic variant within SCN10A modulates cardiac SCN5A expression. *J. Clin. Invest.*, **124**, 1844–1852.
12. Copeland, N.G., Jenkins, N.A. and Court, D.L. (2001) Recombineering: a powerful new tool for mouse functional genomics. *Nat. Rev. Genet.*, **2**, 769–779.
13. Giraldo, P., Gimenez, E. and Montoliu, L. (1999) The use of yeast artificial chromosomes in transgenic animals: expression studies of the tyrosinase gene in transgenic mice. *Genet. Anal.*, **15**, 175–178.
14. Schedl, A., Beermann, F., Thies, E., Montoliu, L., Kelsey, G. and Schutz, G. (1992) Transgenic mice generated by pronuclear injection of a yeast artificial chromosome. *Nucleic Acids Res.*, **20**, 3073–3077.
15. Van Keuren, M.L., Gavrilina, G.B., Filipiak, W.E., Zeidler, M.G. and Saunders, T.L. (2009) Generating transgenic mice from bacterial artificial chromosomes: transgenesis efficiency, integration and expression outcomes. *Transgenic Res.*, **18**, 769–785.
16. Feng, D.X., Liu, D.P., Huang, Y., Wu, L., Li, T.C., Wu, M., Tang, X.B. and Liang, C.C. (2001) The expression of human alpha-like globin genes in transgenic mice mediated by bacterial artificial chromosome. *Proc. Natl. Acad. Sci. U.S.A.*, **98**, 15073–15077.
17. Giraldo, P. and Montoliu, L. (2002) Artificial chromosome transgenesis in pigmentary research. *Pigment Cell Res.*, **15**, 258–264.
18. Moreira, P.N., Giraldo, P., Cozar, P., Pozueta, J., Jimenez, A., Montoliu, L. and Gutiérrez-Adán, A. (2004) Efficient generation of transgenic mice with intact yeast artificial chromosomes by intracytoplasmic sperm injection. *Biol. Reprod.*, **71**, 1943–1947.
19. Birbach, A., Casanova, E. and Schmid, J.A. (2009) A Probasin-MerCreMer BAC allows inducible recombination in the mouse prostate. *Genesis*, **47**, 757–764.
20. Beil, J., Fairbairn, L., Pelczar, P. and Buch, T. (2012) Is BAC transgenesis obsolete? State of the art in the era of designer nucleases. *J. Biomed. Biotechnol.*, **2012**, 308414.
21. Harris, J.A., Hirokawa, K.E., Sorensen, S.A., Gu, H., Mills, M., Ng, L.L., Bohn, P., Mortrud, M., Ouellette, B., Kidney, J. *et al.* (2014) Anatomical characterization of Cre driver mice for neural circuit mapping and manipulation. *Front. Neural Circuits*, **8**, 76.
22. Andrey, G., Montavon, T., Mascres, B., Gonzalez, F., Noordermeer, D., Leleu, M., Trono, D., Spitz, F. and Duboule, D. (2013) A switch between topological domains underlies HoxD genes collinearity in mouse limbs. *Science*, **340**, 1234167.
23. Reid, L.H., Shesely, E.G., Kim, H.S. and Smithies, O. (1991) Cotransformation and gene targeting in mouse embryonic stem cells. *Mol. Cell. Biol.*, **11**, 2769–2777.
24. Sagai, T., Hosoya, M., Mizushima, Y., Tamura, M. and Shiroishi, T. (2005) Elimination of a long-range cis-regulatory module causes complete loss of limb-specific Shh expression and truncation of the mouse limb. *Development*, **132**, 797–803.
25. Bender, M.A., Byron, R., Ragoczy, T., Telling, A., Bulger, M. and Groudine, M. (2006) Flanking HS-62.5 and 3' HS1, and regions upstream of the LCR, are not required for beta-globin transcription. *Blood*, **108**, 1395–1401.
26. Visel, A., Zhu, Y., May, D., Afzal, V., Gong, E., Attanasio, C., Blow, M.J., Cohen, J.C., Rubin, E.M. and Pennacchio, L.A. (2010) Targeted deletion of the 9p21 non-coding coronary artery disease risk interval in mice. *Nature*, **464**, 409–412.
27. Balasubramani, A., Winstead, C.J., Turner, H., Janowski, K.M., Harbour, S.N., Shibata, Y., Crawford, G.E., Hatton, R.D. and Weaver, C.T. (2014) Deletion of a conserved cis-element in the Ifng locus highlights the role of acute histone acetylation in modulating inducible gene transcription. *PLoS Genet.*, **10**, e1003969.
28. Ishii, A., Kurosawa, A., Saito, S. and Adachi, N. (2014) Analysis of the role of homology arms in gene-targeting vectors in human cells. *PLoS One*, **9**, e108236.
29. Giraldo, P., Martinez, A., Regales, L., Lavado, A., Garcia-Diaz, A., Alonso, A., Busturia, A. and Montoliu, L. (2003) Functional dissection of the mouse tyrosinase locus control region identifies a new putative boundary activity. *Nucleic Acids Res.*, **31**, 6290–6305.
30. Doudna, J.A. and Charpentier, E. (2014) Genome editing. The new frontier of genome engineering with CRISPR-Cas9. *Science*, **346**, 1258096.
31. Seruggia, D. and Montoliu, L. (2014) The new CRISPR-Cas system: RNA-guided genome engineering to efficiently produce any desired genetic alteration in animals. *Transgenic Res.*, **23**, 707–716.
32. Jinek, M., Chylinski, K., Fonfara, I., Hauer, M., Doudna, J.A. and Charpentier, E. (2012) A programmable dual-RNA-guided DNA endonuclease in adaptive bacterial immunity. *Science*, **337**, 816–821.
33. Wang, H., Yang, H., Shivalila, C.S., Dawlaty, M.M., Cheng, A.W., Zhang, F. and Jaenisch, R. (2013) One-step generation of mice carrying mutations in multiple genes by CRISPR/Cas-mediated genome engineering. *Cell*, **153**, 910–918.
34. Fujii, W., Kawasaki, K., Sugiura, K. and Naito, K. (2013) Efficient generation of large-scale genome-modified mice using gRNA and CAS9 endonuclease. *Nucleic Acids Res.*, **41**, e187.
35. Lavado, A. and Montoliu, L. (2006) New animal models to study the role of tyrosinase in normal retinal development. *Front. Biosci.*, **11**, 743–752.
36. Olivares, C. and Solano, F. (2009) New insights into the active site structure and catalytic mechanism of tyrosinase and its related proteins. *Pigment Cell Melanoma Res.*, **22**, 750–760.
37. Gimenez, E., Lavado, A., Giraldo, P. and Montoliu, L. (2003) Tyrosinase gene expression is not detected in mouse brain outside the retinal pigment epithelium cells. *Eur. J. Neurosci.*, **18**, 2673–2676.
38. Montoliu, L., Gronskov, K., Wei, A.H., Martinez-Garcia, M., Fernandez, A., Arveiler, B., Morice-Picard, F., Riazuddin, S., Suzuki, T., Ahmed, Z.M. *et al.* (2014) Increasing the complexity: new genes and new types of albinism. *Pigment Cell Melanoma Res.*, **27**, 11–18.
39. Ganss, R., Montoliu, L., Monaghan, A.P. and Schutz, G. (1994) A cell-specific enhancer far upstream of the mouse tyrosinase gene confers high level and copy number-related expression in transgenic mice. *EMBO J.*, **13**, 3083–3093.
40. Bessa, J., Tena, J.J., de la Calle-Mustienes, E., Fernandez-Minan, A., Naranjo, S., Fernandez, A., Montoliu, L., Akalin, A., Lenhard, B., Casares, F. *et al.* (2009) Zebrafish enhancer detection (ZED) vector: a new tool to facilitate transgenesis and the functional analysis of cis-regulatory regions in zebrafish. *Dev. Dyn.*, **238**, 2409–2417.

41. Harms, D.W., Quadros, R.M., Seruggia, D., Ohtsuka, M., Takahashi, G., Montoliu, L. and Gurumurthy, C.B. (2014) Mouse genome editing using the CRISPR/Cas system. *Curr. Protoc. Hum. Genet.*, **83**, 15.7.1–15.7.27.
42. Gorkin, D.U., Lee, D., Reed, X., Fletez-Brant, C., Bessling, S.L., Loftus, S.K., Beer, M.A., Pavan, W.J. and McCallion, A.S. (2012) Integration of ChIP-seq and machine learning reveals enhancers and a predictive regulatory sequence vocabulary in melanocytes. *Genome Res.*, **22**, 2290–2301.
43. Furlan-Magaril, M., Rebollar, E., Guerrero, G., Fernandez, A., Molto, E., Gonzalez-Buendia, E., Cantero, M., Montoliu, L. and Recillas-Targa, F. (2011) An insulator embedded in the chicken alpha-globin locus regulates chromatin domain configuration and differential gene expression. *Nucleic Acids Res.*, **39**, 89–103.
44. Wasmeier, C., Romao, M., Plowright, L., Bennett, D.C., Raposo, G. and Seabra, M.C. (2006) Rab38 and Rab32 control post-Golgi trafficking of melanogenic enzymes. *J. Cell Biol.*, **175**, 271–281.
45. Montoliu, L. (2012) Mendel: a simple excel workbook to compare the observed and expected distributions of genotypes/phenotypes in transgenic and knockout mouse crosses involving up to three unlinked loci by means of a chi2 test. *Transgenic Res.*, **21**, 677–681.
46. Canver, M.C., Bauer, D.E., Dass, A., Yien, Y.Y., Chung, J., Masuda, T., Maeda, T., Paw, B.H. and Orkin, S.H. (2014) Characterization of genomic deletion efficiency mediated by clustered regularly interspaced palindromic repeats (CRISPR)/Cas9 nuclease system in mammalian cells. *J. Biol. Chem.*, **289**, 21312–21324.
47. Xiao, A., Wang, Z., Hu, Y., Wu, Y., Luo, Z., Yang, Z., Zu, Y., Li, W., Huang, P., Tong, X. *et al.* (2013) Chromosomal deletions and inversions mediated by TALENs and CRISPR/Cas in zebrafish. *Nucleic Acids Res.*, **41**, e141.
48. Porter, S., Larue, L. and Mintz, B. (1991) Mosaicism of tyrosinase-locus transcription and chromatin structure in dark vs. light melanocyte clones of homozygous chinchilla-mottled mice. *Dev. Genet.*, **12**, 393–402.
49. Lavado, A., Olivares, C., Garcia-Borrón, J.C. and Montoliu, L. (2005) Molecular basis of the extreme dilution mottled mouse mutation: a combination of coding and noncoding genomic alterations. *J. Biol. Chem.*, **280**, 4817–4824.
50. Parikh, B.A., Beckman, D.L., Patel, S.J., White, J.M. and Yokoyama, W.M. (2015) Detailed phenotypic and molecular analyses of genetically modified mice generated by CRISPR-Cas9-mediated editing. *PLoS One*, **10**, e0116484.
51. Fu, Y., Foden, J.A., Khayter, C., Maeder, M.L., Reyon, D., Joung, J.K. and Sander, J.D. (2013) High-frequency off-target mutagenesis induced by CRISPR-Cas nucleases in human cells. *Nat. Biotechnol.*, **31**, 822–826.
52. Mali, P., Aach, J., Stranges, P.B., Esvelt, K.M., Moosburner, M., Kosuri, S., Yang, L. and Church, G.M. (2013) CAS9 transcriptional activators for target specificity screening and paired nickases for cooperative genome engineering. *Nat. Biotechnol.*, **31**, 833–838.
53. Pattanayak, V., Lin, S., Guilinger, J.P., Ma, E., Doudna, J.A. and Liu, D.R. (2013) High-throughput profiling of off-target DNA cleavage reveals RNA-programmed Cas9 nuclease specificity. *Nat. Biotechnol.*, **31**, 839–843.
54. Regales, L., Giraldo, P., Garcia-Diaz, A., Lavado, A. and Montoliu, L. (2003) Identification and functional validation of a 5' upstream regulatory sequence in the human tyrosinase gene homologous to the locus control region of the mouse tyrosinase gene. *Pigment Cell Res.*, **16**, 685–692.
55. King, R.A., Pietsch, J., Fryer, J.P., Savage, S., Brott, M.J., Russell-Eggitt, I., Summers, C.G. and Oetting, W.S. (2003) Tyrosinase gene mutations in oculocutaneous albinism 1 (OCA1): definition of the phenotype. *Hum. Genet.*, **113**, 502–513.
56. Rooryck, C., Morice-Picard, F., Elcioglu, N.H., Lacombe, D., Taieb, A. and Arveiler, B. (2008) Molecular diagnosis of oculocutaneous albinism: new mutations in the OCA1–4 genes and practical aspects. *Pigment Cell Melanoma Res.*, **21**, 583–587.
57. Molto, E., Fernandez, A. and Montoliu, L. (2009) Boundaries in vertebrate genomes: different solutions to adequately insulate gene expression domains. *Brief. Funct. Genomic Proteomic*, **8**, 283–296.
58. Roman, A.C., Gonzalez-Rico, F.J., Molto, E., Hernando, H., Neto, A., Vicente-Garcia, C., Ballestar, E., Gómez-Skarmeta, J.L., Vavrova-Anderson, J., White, R.J. *et al.* (2011) Dioxin receptor and SLUG transcription factors regulate the insulator activity of B1 SINE retrotransposons via an RNA polymerase switch. *Genome Res.*, **21**, 422–432.
59. Martin, D., Pantoja, C., Fernandez Minan, A., Valdes-Quezada, C., Molto, E., Matesanz, F., Bogdanović, O., de la Calle-Mustienes, E., Domínguez, O., Taher, L. *et al.* (2011) Genome-wide CTCF distribution in vertebrates defines equivalent sites that aid the identification of disease-associated genes. *Nat. Struct. Mol. Biol.*, **18**, 708–714.
60. Tiana, M., Villar, D., Perez-Guijarro, E., Gomez-Maldonado, L., Molto, E., Fernandez-Minan, A., Gómez-Skarmeta, J.L., Montoliu, L. and del Peso, L. (2012) A role for insulator elements in the regulation of gene expression response to hypoxia. *Nucleic Acids Res.*, **40**, 1916–19127.
61. Lim, S., Wang, Y., Yu, X., Huang, Y., Featherstone, M.S. and Sampath, K. (2013) A simple strategy for heritable chromosomal deletions in zebrafish via the combinatorial action of targeting nucleases. *Genome Biol.*, **14**, R69.
62. Mansour, M.R., Abraham, B.J., Anders, L., Berezovskaya, A., Gutierrez, A., Durbin, A.D., Etchin, J., Lawton, L., Sallan, S.E., Silverman, L.B. *et al.* Oncogene regulation. An oncogenic super-enhancer formed through somatic mutation of a noncoding intergenic element. *Science*, **346**, 1373–1377.
63. Kraft, K., Geuer, S., Will, A.J., Chan, W.L., Paliou, C., Borschiwer, M., Harabula, I., Wittler, L., Franke, M., Ibrahim, D.M. *et al.* (2015) Deletions, inversions, duplications: engineering of structural variants using CRISPR/Cas in mice. *Cell Rep.*, doi:10.1016/j.celrep.2015.01.016.
64. Murisier, F., Guichard, S. and Beermann, F. (2007) Distinct distal regulatory elements control tyrosinase expression in melanocytes and the retinal pigment epithelium. *Dev. Biol.*, **303**, 838–847.
65. Schedl, A., Montoliu, L., Kelsey, G. and Schutz, G. (1993) A yeast artificial chromosome covering the tyrosinase gene confers copy number-dependent expression in transgenic mice. *Nature*, **362**, 258–261.
66. Bauer, D.E., Kamran, S.C., Lessard, S., Xu, J., Fujiwara, Y., Lin, C., Shao, Z., Canver, M.C., Smith, E.C., Pinello, L. *et al.* (2013) An erythroid enhancer of BCL11A subject to genetic variation determines fetal hemoglobin level. *Science*, **342**, 253–257.
67. Xu, J., Shao, Z., Li, D., Xie, H., Kim, W., Huang, J., Taylor, J.E., Pinello, L., Glass, K., Jaffe, J.D. *et al.* (2015) Developmental control of polycomb subunit composition by GATA factors mediates a switch to non-canonical functions. *Mol. Cell*, **57**, 304–316.
68. Lavado, A., Matheu, A., Serrano, M. and Montoliu, L. (2005) A strategy to study tyrosinase transgenes in mouse melanocytes. *BMC Cell Biol.*, **6**, 18.